Comparison of Planetary Hα-emission Models: A New Correlation with Accretion Luminosity

Yuhiko Aoyama[1,2,3,9] , Gabriel-Dominique Marleau[4,5,6] , Masahiro Ikoma[3,7,8] , and Christoph Mordasini[5]
[1] Institute for Advanced Study, Tsinghua University, Beijing 100084, People's Republic of China; yaoyama@tsinghua.edu.cn
[2] Department of Astronomy, Tsinghua University, Beijing 100084, People's Republic of China
[3] Department of Earth and Planetary Science, The University of Tokyo, 7-3-1 Hongo, Bunkyo-ku, Tokyo 113-0033, Japan
[4] Institut für Astronomie und Astrophysik, Universität Tübingen, Auf der Morgenstelle 10, D-72076 Tübingen, Germany
[5] Physikalisches Institut, Universität Bern, Gesellschaftsstr. 6, 3012 Bern, Switzerland
[6] Max-Planck-Institut für Astronomie, Königstuhl 17, D-69117 Heidelberg, Germany
[7] Division of Science, National Astronomical Observatory of Japan, 2-21-1 Osawa, Mitaka, Tokyo 181-8588, Japan
[8] Department of Astronomical Science, The Graduate University for Advanced Studies, SOKENDAI, 2-21-1 Osawa, Mitaka, Tokyo 181-8588, Japan

Abstract

Accreting planets have been detected through their hydrogen-line emission, specifically Hα. To interpret this, stellar-regime empirical correlations between the Hα luminosity $L_{H\alpha}$ and the accretion luminosity L_{acc} or accretion rate $\dot{M}$ have been extrapolated to planetary masses, however without validation. We present a theoretical L_{acc}–$L_{H\alpha}$ relationship applicable to a shock at the surface of a planet. We consider wide ranges of accretion rates and masses and use detailed spectrally resolved, nonequilibrium models of the postshock cooling. The new relationship gives a markedly higher L_{acc} for a given $L_{H\alpha}$ than fits to young stellar objects, because Lyα, which is not observable, carries a large fraction of L_{acc}. Specifically, an $L_{H\alpha}$ measurement needs 10 to 100 times higher L_{acc} and $\dot{M}$ than previously predicted, which may explain the rarity of planetary Hα detections. We also compare the $\dot{M}$–$L_{H\alpha}$ relationships coming from the planet-surface shock or implied by accretion-funnel emission. Both can contribute simultaneously to an observed Hα signal, but at low (high) $\dot{M}$ the planetary-surface shock (heated funnel) dominates. Only the shock produces Gaussian line wings. Finally, we discuss accretion contexts in which different emission scenarios may apply, putting recent literature models in perspective, and also present L_{acc}–L_{line} relationships for several other hydrogen lines.

1. Introduction

Recent observations have detected Hα emission from planets around young accreting stars (Wagner et al. 2018; Haffert et al. 2019, hereafter H19; Eriksson et al. 2020; Hashimoto et al. 2020). For stars, sufficiently strong Hα indicates gas accretion (Hartmann et al. 2016), and empirical relationships between Hα luminosity and accretion luminosity exist, where the latter is estimated from UV continuum observations (e.g., Fang et al. 2009). Because initially no $L_{H\alpha}$–L_{acc} correlations were available for the planetary case, these stellar scalings have been extrapolated to analyze individual detections or surveys results (Sallum et al. 2015; Wagner et al. 2018; H19; Cugno et al. 2019; Xie et al. 2020; Zurlo et al. 2020). However, verifying whether these correlations hold also at planetary masses was not yet possible.

Following the reports on planetary Hα detection, theoretical work has attempted to reproduce and interpret the observations. Thanathibodee et al. (2019, hereafter Th19) applied a magnetospheric accretion model developed for T Tauri stars (Muzerolle et al. 2001) to planetary masses and radii, and could reproduce the Hα line of PDS 70 b. They assumed a strong magnetic field able to truncate the accretion disk (Christensen et al. 2009; Batygin 2018) and hot gas ($T \sim 10^4$ K) in the accretion funnel.

In another direction, Aoyama et al. (2018, hereafter AIT18) constructed the first emission model of *shock*-heated gas for

planetary masses, focusing on hydrogen lines. There, the Hα comes from the postshock gas and not the accretion flow. This can reproduce the observations if a strong shock of preshock velocity $v \gtrsim 30\,km\,s^{-1}$ occurs on the circumplanetary disk (CPD) surface or on the planetary surface (Aoyama & Ikoma 2019, hereafter AI19). The former is suggested by isothermal 3D hydrodynamic simulations (Tanigawa et al. 2012), in which the gas flows almost vertically in freefall onto the CPD. A planetary-surface shock can occur when the gas falls directly from the upper layers of the protoplanetary disk (PPD), for instance, from meridional circulation (Szulágyi et al. 2014; Teague et al. 2019) or through magnetospheric accretion columns originating at the inner edge of the CPD (e.g., Lovelace et al. 2011; Batygin 2018). Such flow patterns need nonisothermal or magnetic effects, respectively.

In this Letter, we derive new theoretical L_{acc}–$L_{H\alpha}$ and $\dot{M}$–$L_{H\alpha}$ relationships from our shock emission model for planetary-surface accretion.[10] We compare them with correlations measured for stars. Afterward, we discuss the differences among theoretical models and predictions, including Szulágyi & Ercolano (2020, hereafter SzE20). We also comment in Appendix B on the $L_{H\alpha}$ estimate by Zhu (2015), and present correlations for several other lines in Appendix C.

---

[10] Contrary to statements in the literature, in AIT18 the line flux is not intrinsically high; it depends on the input parameters. Also, the $T \sim 10^4$–10^6 K in AIT18 are not effective temperatures but rather part of nonequilibrium cooling in a thin postshock layer (roughly the Zel'dovich spike).
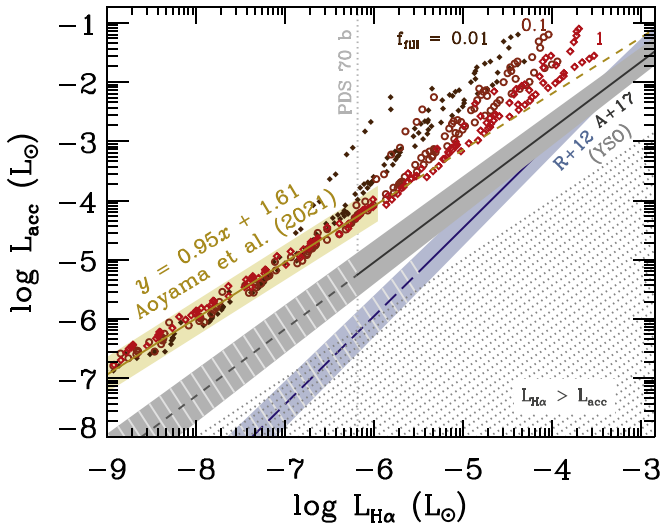
Figure 1. Theoretical relationships between accretion luminosity, $L_{\rm acc}$, and Hα luminosity, $L_{\rm H\alpha}$. The symbols show our model results for a wide range of accretion rates $\dot{M} = 3 \times 10^{-10}$–$3 \times 10^{-5} M_{\rm J}$ yr^{-1} and masses $M_{\rm p} = 2$–$20 M_{\rm J}$, with filling factor $f_{\rm fill} = 0.01$ (filled diamonds), 0.1 (circles), and 1 (open diamonds). The golden line indicates Equation (1), which fits our results up to $\log(L_{\rm acc}/L_\odot) = -4$; the dashed line is an extrapolation. The shaded golden region shows the spread $\pm \sigma = \pm 0.3$ dex. Fits by Rigliaco et al. (2012, blue) and Alcalá et al. (2017, gray) for stellar-mass objects are also shown by the blue and gray lines, respectively. The shaded regions reflect the formal errors (Equation (A1)), with $\sigma_{\log L_{\rm H\alpha}} = 0$, which correspond to the usual approach but ignore the spread of their data ($\pm \sigma \approx \pm 0.5$–$0.7$ dex). The dashed lines indicate extrapolations. Extinction by material around the planet (not included) would only move the points to the left, away from the stellar relationships. Already without considering extinction, our relationship differs clearly from the stellar fits, by up to 2.5 dex here. The dotted region has $L_{\rm H\alpha} > L_{\rm acc}$, which could be unlikely (see the text).

2. Stellar and Planetary Accretion Relationships

2.1. Comparison of L_{acc}–$L_{H\alpha}$ Relationships

In stellar observations, UV/optical continuum measurements (e.g., Gullbring et al. 1998) have been used to estimate the accretion luminosity $L_{\rm acc}$ by modeling the emission from the shock-heated photosphere (e.g., Calvet & Gullbring 1998). However, for distant objects, interstellar extinction prevents the detection of such continua. On the other hand, Hα is brighter and less extincted. Thus, empirical $L_{\rm acc}$–$L_{\rm H\alpha}$ relationships derived for nearby stars are used to estimate $L_{\rm acc}$ from the observed $L_{\rm H\alpha}$. Then, assuming a mass and radius or using known estimates from photometry, $\dot{M}$ is estimated for distant accretors.

In Figure 1, we show the $L_{\rm acc}$–$L_{\rm H\alpha}$ correlation from AI19's models, detailed in Aoyama et al. (2020, hereafter AMMI21). They simulated the radiative transfer of hydrogen lines in the 1D plane-parallel flow of the shock-heated gas. Since the timescale of temperature change is comparable to that of line emission process, they numerically calculated the time-evolving electron transitions via collision and radiation. This model estimates the hydrogen line intensity for two input parameters of preshock gas velocity v_0 and number density n_0. Assuming the accreting gas falls onto the planetary surface with the freefall velocity, the model estimates the hydrogen line luminosity as a function of the planetary mass $M_{\rm p}$ and the accretion rate $\dot{M}$. As in AMMI21, $L_{\rm acc} = GM_{\rm p}\dot{M}(R_{\rm p}^{-1} - R_{\rm in}^{-1})$, where G is the gravitational constant, $R_{\rm p}$ is the planetary radius, and $R_{\rm in}$ is the radius from which the gas starts at rest. We consider a wide range of mass accretion rates $\dot{M} = 3 \times 10^{-10}$

$-3 \times 10^{-5} M_{\rm J}$ yr^{-1} and masses $M_{\rm p} = 2$–$20 M_{\rm J}$, and consider a filling factor $f_{\rm fill} = 0.01$, 0.1, or 1, where the Hα emission comes from the area of the shock of $f_{\rm fill} 4\pi R_{\rm p}^2$. For $f_{\rm fill} = 1$, $R_{\rm in} = \infty$ (since $R_{\rm in} \approx 1/4 R_{\rm Hill} \gg R_{\rm p}$, where $R_{\rm Hill}$ is the Hill radius; Mordasini et al. 2012), and $R_{\rm in} = 5 R_{\rm p}$ for $f_{\rm fill} \leqslant 0.1$ as for magnetospheric accretion (Hartmann et al. 2016). We use fits by AMMI21 of $R_{\rm p}(\dot{M}, M_{\rm p})$ from the Mordasini et al. (2012) planet-structure model, which predicts $R_{\rm p} \approx 1.5$–$5 R_{\rm J}$.

For $L_{\rm acc} \lesssim 10^{-4} L_\odot$, $L_{\rm acc}$ and $L_{\rm H\alpha}$ correlate well with each other.[11] The spread in $L_{\rm acc}$ ($\lesssim 1.5$ dex) at higher $L_{\rm acc}$ reflects the large optical depth at Hα. In high-$L_{\rm acc}$ (or higher-density) cases, Hα from optically thick regions hardly escapes, and other lines take over the energy transfer. Decreasing $f_{\rm fill}$ increases the (preshock) postshock density and thus the postshock optical thickness (AIT18). Thus, decreasing $f_{\rm fill}$ also increases $L_{\rm acc}$ at a given $L_{\rm H\alpha}$, and $f_{\rm fill} = 1$ yields the minimal $L_{\rm acc}$ for a given $L_{\rm H\alpha}$. Also, lower masses sit toward higher $L_{\rm acc}$ for a given $L_{\rm H\alpha}$ because v_0 is lower, causing a lower excitation degree and less effective hydrogen line emission.

We fit our $L_{\rm acc}$–$L_{\rm H\alpha}$ relationship in the form of $y = ax + b$ for $L_{\rm acc} \leqslant 10^{-4} L_\odot$:

$$\log_{10}(L_{\rm acc}/L_\odot) = 0.95 \times \log_{10}(L_{\rm H\alpha}/L_\odot) + 1.61, \qquad (1)$$

where $L_\odot = 3.84 \times 10^{26}$ erg s^{-1}. The upward spread due to high optical depths barely affects the fit because optically thin cases are much more frequent for a uniform sampling of $M_{\rm p}$ and $\dot{M}$. The formal error bars are $\sigma_a = 0.006$ and $\sigma_b = 0.04$, with the residual rms $= 0.11$ dex, but the half-spread at a given $L_{\rm H\alpha}$ is $\sigma \approx 0.3$ dex (shaded region in Figure 1). We recommend using $\sigma = 0.30$ as the uncertainty when determining $L_{\rm acc}$ from $L_{\rm H\alpha}$ and propagating errors (Appendix A).

We compare our fit to two empirical relationships derived for stars. The blue region in Figure 1 shows the relationship of Rigliaco et al. (2012, hereafter R12). To explain a given $L_{\rm H\alpha}$, R12's fit requires an $L_{\rm acc}$ smaller than our estimate by up to two orders of magnitude. Since, in the shock model, the accretion energy is partitioned into the Lyα emission more by a factor of several tens than into the Hα emission, such a high $L_{\rm H\alpha}/L_{\rm acc}$ ratio cannot be achieved. In contrast, in the magnetospheric accretion model used for interpreting the Hα emission in the stellar regime, Lyα emission should be less efficient than in the planetary shock model due to, for example, large optical thickness. Also, we note that a part of stellar Hα energy (i.e., the energy heating the accretion column) might come from the stellar interior energy through the magnetic field, in addition to the accretion energy. R12's fit also differs greatly in slope from ours. This is because R12's empirical relationship was derived using stellar objects of higher $\dot{M}$ (or $L_{\rm acc}$) than studied here; for more massive stars, more energy is emitted in the UV continuum rather than in optical lines such as Hα (Zhou et al. 2014). This is also the reason why the $L_{\rm acc}$ estimated in Zhou et al. (2021) via UV continuum is lower than ours. For stellar cases with stronger shock, Lyα should be much weaker than UV continuum and negligible, and $L_{\rm acc}$ is well estimated only via UV continuum. But in the planetary shock emission, Lyα carries a large fraction of the energy, while this line is not observable due to strong circumstellar extinction. Even at TW Hya, one of the closest young stellar objects, the interstellar hydrogen column density is $\approx 10^{19.5}$ cm^{-2} (Herczeg et al. 2004). Combined with the narrowness of the planetary Lyα

---

[11] Or for $L_{\rm H\alpha} \lesssim 10^{-5.5} L_\odot$ at $f_{\rm fill} \gtrsim 0.3$ and $L_{\rm H\alpha} \lesssim 10^{-6.5} L_\odot$ for all $f_{\rm fill}$.

line for low planet masses (full width at half-maximum $\sim$0.3 Å), this lets at most a percent of the Lyα reach us (Landsman & Simon 1993). Thus, the flux ratio of Lyα to Hα is around 0.1 or likely less, even at such a favorable target. For an object of $\gtrsim$20 M_J, roughly 10 times more Lyα passes through the interstellar medium (ISM) due to the greater line width.

Also, for $L_{H\alpha} \lesssim 10^{-6} L_\odot$, R12's extrapolated fit suggests $L_{H\alpha} > L_{acc}$: more energy is emitted in Hα than is brought in by the accreting gas. This is not necessarily unphysical, since the Hα does not have to originate from the accretion shock, but seems unlikely since here the only other energy source is the interior luminosity (usually smaller than L_{acc}; Mordasini et al. 2017).

The gray band in Figure 1 is from Alcalá et al. (2017, hereafter Al17), who extended the sample of Alcalá et al. (2014). Since Al17 fit only to very-low-mass stars, their slope should apply to planets presumably better more than R12. However, also Al17's fitted line differs from ours by an order of magnitude. This reflects the contrasting Hα emission mechanisms. Our model calculates Hα from the shock-heated gas, while the stellar Hα is thought to come (mainly) from an accretion funnel (Hartmann et al. 2016). Section 3.1 discusses this more extensively.

Our L_{acc}–$L_{H\alpha}$ relationship yields a higher L_{acc}, for an observed $L_{H\alpha}$, than both Al17, $y = 1.13x + 1.74$, and shallower R12, $y = 1.49x + 2.99$ do. Our curve also lies above those stellar correlations. Therefore, a measurement of (or upper limit on) $L_{H\alpha}$ corresponds to a much higher accretion luminosity than inferred from the stellar fits. Since $\dot{M}$ is unknown within several orders of magnitude, whereas the mass and radius uncertainties are much smaller, L_{acc} should be set mostly by $\dot{M}$. Thus, an observed $L_{H\alpha}$ corresponds to a higher $\dot{M}$ than inferred previously, suggesting that only strong accretors produce Hα bright enough for detection. This might help explain the low yields of recent Hα surveys (Cugno et al. 2019; Xie et al. 2020; Zurlo et al. 2020).

In Figure 1, a range of $L_{H\alpha}$ values is covered both by the Al17 data and our model points (especially for $f_{fill} \gtrsim 0.1$), at $L_{H\alpha} \gtrsim 5 \times 10^{-7} L_\odot$. The two are separated by 1–2.5 dex at a given $L_{H\alpha}$. However, the emission mechanisms likely differ (Section 3). Therefore, the two relationships need not match. Also, if at a given L_{acc} there are contributions from the shock and the accretion column, the latter probably dominates at high $\dot{M}$ (Section 2.2). If however the temperature in the accretion column is below $T \approx 10^4$ K or $\dot{M}$ is low, the surface shock more likely dominates.

Figure 1 shows the observed $L_{H\alpha}$ value of PDS 70 b (vertical dotted line; Zhou et al. 2021) as a typical planetary $L_{H\alpha}$ (see PDS 70 c and Delorme 1 (AB)b; Haffert et al. 2019; Eriksson et al. 2020). Our fit implies $L_{acc} \approx 5 \times 10^{-5} L_\odot$, which is respectively about 10 and 100 times larger than for Al17 and R12, with the latter in the $L_{H\alpha} > L_{acc}$ region.[12] Our predicted L_{acc} is a lower limit if, as Hashimoto et al. (2020) infer, there is extinction.

2.2. Comparison of $\dot{M}$–$L_{H\alpha}$ Relationships

A common approach in the literature is to use empirical $\dot{M}$–$L_{H\alpha}$ correlations to infer $\dot{M}$. This approach hides the possibly
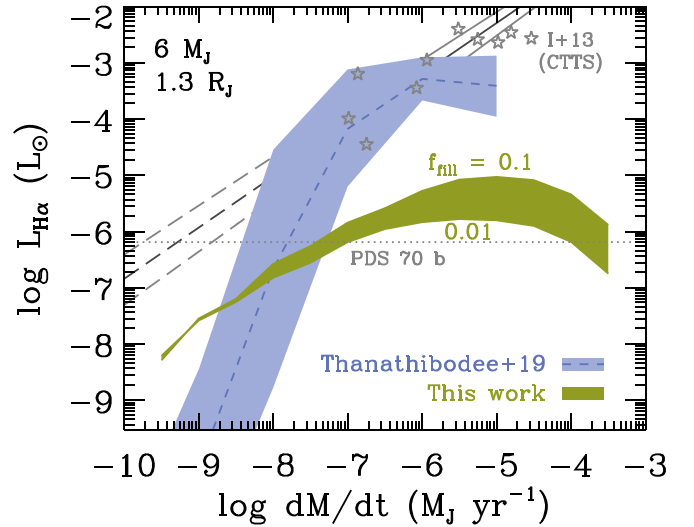
Figure 2. Restricted comparison of the $\dot{M}$–$L_{H\alpha}$ relations for fixed $M_p = 6 \, M_J$ and $R_p = 1.3 \, R_J$ (only here) from Thanathibodee et al. (2019, blue band: 1σ) and this work (green band). The bottom (top) border of our region is for $f_{fill} = 0.01$ (0.1), with Th19 finding $f_{fill} = 0.01$–0.1. Gray stars and lines show the Ingleby et al. (2013) data and fit ($\pm\sigma$) for CTTSs ($M \approx M_\odot$) for comparison. PDS 70 b is highlighted (gray dotted line; Zhou et al. 2021). For a version of this figure with extinction, see Marleau et al. (2021).

complex dependence of $L_{H\alpha}$ on several parameters into a best-fitting coefficient. Nevertheless, it is useful because $\dot{M}$ can vary by several orders of magnitude between objects, while M_p/R_p vary by much less, with $L_{H\alpha}$ correlating with $L_{acc} \propto M_p\dot{M}/R_p$ roughly.

We present in Figure 2 our $\dot{M}$–$L_{H\alpha}$ relationship. To compare to Th19, we fix $M_p = 6 \, M_J$ and $R_p = 1.3 \, R_J$. Since Th19 assume magnetospheric accretion, we take $f_{fill} = 0.1$ and 0.01. Figure 2 shows that the dependence of $L_{H\alpha}$ on $\dot{M}$ differs greatly between the surface shock (this work) and the heated accretion column Th19. The latter has some overlap with the classical T Tauri star (CTTS) relationship of Ingleby et al. (2013), who fitted higher-mass objects than R12. Both in Th19 and here no extinction is considered. In our shock model, the emitted $L_{H\alpha}$ less steeply depends on the $\dot{M}$ relative to the model of Th19.

The key point of Figure 2 is that the emission from the heated accretion column and that from the surface shock dominate in different regimes. Below a crossover value $\dot{M}_{cross}$, the surface shock yields most of the Hα luminosity, whereas at $\dot{M} \gtrsim \dot{M}_{cross}$ the accretion column dominates. The Th19 models were fitted to a specific observation of a single object, and we too considered only one (M_p, R_p) combination here. While $\dot{M}_{cross}$ presumably depends on these parameters, the qualitative result that there is an $\dot{M}_{cross}$ should be general.

If planets accrete mostly at $\dot{M} > \dot{M}_{cross}$, the surface shock will not dominate $L_{H\alpha}$. However, it is unclear how high $\dot{M}/\dot{M}_{cross}$ can be. For PDS 70 b, Th19 fit a maximum temperature in the accretion column $T_{max} \approx 10^4$ K. If T_{max} is significantly lower because accretion is less energetic for planets,[13] $\dot{M}_{cross}$ could become very high and thus irrelevant in practice and the shock emission would dominate the $L_{H\alpha}$. Also, it has not (yet) been shown that magnetospheric accretion onto planets can occur at all. Finally, if planets have short phases of

---

[12] When Wagner et al. (2018) used R12's fit, L_{acc} was larger than $L_{H\alpha}$ because they estimated $L_{H\alpha} = 1.4 \times 10^{-6} L_\odot$ (AMMI21).

[13] Even in energetic accretion by massive objects ($\gtrsim 20 M_J$), the shock still generates hydrogen lines. However, it hardly influences $L_{H\alpha}$ because most energy is emitted at shorter wavelengths (UV and X-ray).

high $\dot{M}$ (e.g., Lubow & Martin 2012; Brittain et al. 2020) but accrete mostly at low $\dot{M} < \dot{M}_{\mathrm{cross}}$ (e.g., Tanigawa & Ikoma 2007), observing them in a phase when the surface shock dominates is more likely.

That both models cross near the $L_{\mathrm{H\alpha}}$ of PDS 70 b seems fortuitous. The only other securely detected accreting planetary-mass objects, PDS 70 c and Delorme 1 (AB)b, are fainter (Haffert et al. 2019; Eriksson et al. 2020). Thus, no planetary-mass observation has yet probed the regime where emission from an accretion column would clearly dominate.

2.3. Which Model Is Appropriate to Estimate $\dot{M}$ from $L_{H\alpha}$?

For planetary-mass objects, neither the shock model nor the magnetospheric accretion model indicate that the empirical relationships derived for accreting stars are applicable for planetary-mass objects. Thus, $\dot{M}$ should rather be estimated by using the relationship presented here or the modeling of planetary magnetospheric accretion as Th19 did. As discussed in Section 2.2, for lower $\dot{M}$ (or lower $L_{\mathrm{H\alpha}}$), the shock-induced emission dominates over that from the magnetospheric accretion, and PDS 70 b is located near the threshold. As of writing, surveys have found no planetary Hα other than PDS 70 b and c (Xie et al. 2020; Zurlo et al. 2020). When Hα emission that was not detected due to its faintness is finally detected, we recommend using our relationship for such lower $L_{\mathrm{H\alpha}}$. For PDS 70 b or planets as bright in Hα as PDS 70 b, we discuss the way to distinguish the Hα source in Section 3.1.

3. Discussion: Comparison of Emission Models

In this section, we discuss which source of Hα is expected for different assumptions, taking the planetary-surface shock as the fiducial case, and address how these mechanisms can be distinguished. Appendix B reviews the upper limit on $L_{\mathrm{H\alpha}}$ by Zhu (2015).

3.1. Hα from Accretion Funnels

An accretion shock is a general and efficient way to heat gas. However, stellar-mass objects have a large freefall velocity $v_{\mathrm{ff}} \approx 300\,\mathrm{km\,s^{-1}}$, which leads to too strong a shock for hydrogen-line emission (Hartmann et al. 2016). Indeed, the shock-heated gas reaches $T \gg 10^5$ K, stifling significant line emission: neutral hydrogen is rare and frequent electron–neutral collisions prevent (hydrogen-line-emitting) radiative cascades. Also, the observed stellar Hα line is wide and comparable with the freefall velocity. Since an unrealistically high temperature ($T \sim 10^7$ K) would be required to explain this width by thermal broadening, the Hα is thought to come from the accreting gas. Namely, strongly magnetized protostars create an inner cavity in their protoplanetary disk and funnel the accreting gas along magnetic field lines (e.g., Gravity Collaboration et al. 2020), with a velocity distribution from $-v_{\mathrm{ff}}$ to $+v_{\mathrm{ff}}$ (back to front side; König 1991). Combined with appropriate radiative structures and inclinations, the mechanical Doppler shift from this velocity distribution can reproduce observed Hα widths (Hartmann et al. 1994).

On the other hand, v_{ff} for planets is much lower than for stars, with $v_{\mathrm{ff}} \approx 100\,\sqrt{M_5/R_2}\,\mathrm{km\,s^{-1}}$ (where $X_n \equiv X/[n\,X_{\mathrm{J}}]$) for planets. Such a shock generates a propitious environment ($T \sim 10^5$ K) for Hα emission AIT18 and can reproduce the observed Hα line width AI19. Therefore, for planetary Hα, the

shock-heated gas is a strong candidate, unlike in the stellar case.

Th19 modeled the Hα from a planetary accretion funnel by extending models of stellar emission (Muzerolle et al. 2001). If such accretion funnels exist for planets, the freefalling gas will be shock-heated at the planetary surface and emit nonnegligible Hα. Then, the observed Hα should be a mixture of two components: from the funnel and from the shock.

Non-Gaussian line wings would suggest a contribution from funnels. In funnel emission, the line broadening comes from the bulk (not thermal) velocity. Therefore, the line is a superposition of narrow ($T \approx 10^4$ K) Gaussians and therefore not necessarily Gaussian. For shock emission, the postshock gas exhibits a range of temperatures and velocities. Thus, the profile is also a superposition of Gaussians, but each component is much wider ($T \gtrsim 10^5$ K). Also, the velocity change in the emitting layers is much less than the highest thermal velocity that determines the widest profile. Therefore, the line is nearly Gaussian, especially in the wings. Self-absorption likely makes the Hα line center non-Gaussian (AIT18), but optically thinner lines from shocks could be completely Gaussian. From funnels, the thinner lines are also non-Gaussian.

The asymmetry across the line center can help to distinguish shock from funnel emission. The shock emission necessarily has a wider red-side profile because of the receding emitting gas, while the funnel emission is freer and can have a broader blue side. Distinguishing this requires resolving the line ($R \gtrsim 10^4$).

Also, it is difficult to make the accretion funnel hot enough to produce observable Hα even in stellar cases (Martin 1996), and the heating mechanism, possibly magnetic in nature, remains an open question. Accordingly, Th19 used a parameterized temperature structure. For young, luminous planets, even though the Christensen et al. (2009) scaling predicts a strong magnetic field, the accretion funnel could have a lower temperature (due somehow to the shallower potential) and emit weaker Hα than in the stellar case. Thus, the emission of Hα by planetary accretion funnels is an interesting but currently difficult-to-assess possibility.

3.2. Hα from a Strong Shock on the CPD Surface

The gas that enters the inner parts of the planetary Hill sphere falls onto the CPD roughly vertically (see, e.g., Schulik et al. 2019, 2020 for $M_{\mathrm{p}} \lesssim 1\,M_{\mathrm{J}}$). Three-dimensional isothermal hydrodynamic simulations showed that the velocity just above the CPD surface is comparable to the freefall velocity (e.g., Tanigawa et al. 2012). Therefore, the shock-heated gas can get hot enough to emit observable Hα (Szulágyi & Mordasini 2017; AIT18). However, in this case, most of the gas falls far from the planet, where Hα emission hardly occurs due to the low freefall velocity of the accreting gas (AIT18; Section 5.2 of AMMI21). Thus, only a small fraction of the accreting gas can contribute to the Hα emission.

Consequently, if the gas entering the Hill sphere undergoes shocks on both the CPD and the planet, the former is likely negligible, unless only a small fraction hits the planet. If the CPD connects continuously to the planetary surface (Owen & Menou 2016; Dong et al. 2020) and/or the CPD gas flows outward rather than toward the planet (Szulágyi et al. 2014), existing models show that the CPD surface shock would be the only Hα source because there would be no strong shock on the

planet. However, to reproduce a given Hα luminosity, the CPD surface shock requires a higher mass influx rate[14] onto the CPD than the planetary-surface shock case, because most of accreting gas hardly contributes to the Hα flux. If the shock is at a large distance above the planet, no strong shock is predicted (see Section 3.3).

In the CPD shock case, the Hα spectral profile is similar to the case of the planetary-surface shock, and it is hard to distinguish the two cases with current instrumental resolution (e.g., $R \approx 2500$ with MUSE/VLT). Instead, most of the gas undergoes a weak shock in the far regions of the CPD, and there is much more cool ($< 10^4$ K) gas, which emits molecular lines, than in the case of the planetary-surface shock. Also, the higher mass influx needed to reproduce a given $L_{H\alpha}$ should lead to a higher temperature for the planetary photosphere and the CPD midplane, making both easier to observe.

3.3. Hα from an Extremely Large Planet

Some global 3D radiative-hydrodynamic simulations for $M_p \sim 1–10 \, M_J$ have obtained a roughly spherically symmetric accretion front $\approx 55 \, R_J$ large in radius (Szulágyi & Mordasini 2017). Interpreted as the planet radius, this size is unexpected at those masses of several Jupiter masses in classical planet modeling. With the density–temperature structure around the gravitational-potential point mass from their simulation, SzE20 integrated the radiative-transfer equation, using the Storey & Hummer (1995, hereafter SH95) emissivities in the source term and the gas and dust opacity in the absorption term. This yielded hydrogen-line luminosities.

We discuss two critical aspects of SzE20's approach:

1. The use of SH95. This model was originally derived in the context of photoionization by, e.g., Wolf–Rayet stars. As detailed in AMMI21, these tables do not apply here mainly because they neglect the ground-state population and, therefore, collisional excitations from that state. Particularly for a moderate shock (e.g., Figures 2 and 3 in AIT18 shows the case of $v_0 = 40 \, \mathrm{km \, s^{-1}}$), the low ionization fraction makes the ground state be the most populated state. This contradicts the assumption of SH95 (see also Section 4 in Hummer & Storey 1987). Thus, line emissivities based on SH95 differ fundamentally from the ones from a direct nonequilibrium calculation.

2. The thickness of the cooling region. For relevant densities, its thickness in our models is (much) less than the planetary radius ($\sim 10^{10}$ cm), as expected. For example, in Figure 6 of AMMI21, the characteristic thickness is 10^7 cm. Currently, our model does not include all coolants, in particular metals; if we did, the region would become even thinner (Aoyama et al. 2018, 2020). In SzE20, however, the grid cells at the shock are at least of order $\sim R_J$, much larger than the physical size of the cooling region. Since the emission of a cell is the product of its volume and emissivity, which depends strongly on temperature, the size of the highest-T cells directly influences SzE20's predicted line intensities. This might explain why, in some of their cases, the Hα line luminosity is much larger than the total accretion luminosity ($L_{H\alpha} \gg L_{acc}$). This means the radiative cooling and emission are not consistently treated.

These points demonstrate that the hydrogen-line emission from a planetary shock cannot be calculated by combining SH95 with the output of radiation-hydrodynamical simulations. Particularly concerning the thickness of the cooling region, this approach could keep the gas temperature high for longer than in reality and lead to an overestimate of the line luminosity. This holds for SzE20 even though their simulations are highly resolved for a global 3D simulation with an impressive dynamic range of $\sim 10^4$ in lengthscale and thus capture the general dynamics. The issue is that 3D simulations necessarily remain low resolution compared to the postshock cooling, which acts on a very different (microphysical) scale than the hydrodynamical processes. This challenge holds for the 1D simulations of Marleau et al. (2017, 2019) too, despite their higher resolution.

A shock at tens of R_J is distinguishable spectroscopically, assuming that any Hα is emitted (which requires $v_{ff} \gtrsim 30 \, \mathrm{km \, s^{-1}}$; AIT18). The Hα profile is narrower than in the other cases (Sections 3.1 and 3.2) because the gas is slower than in an accretion funnel in which the gas accelerates until the planet's surface at a few R_J, and cooler than when heated by a strong shock, for which $T > 10^5$ K. The half-width at half-maximum is narrower than the shock velocity $v_{ff} \leqslant 35 \sqrt{M_{10}/R_{30}} \, \mathrm{km \, s^{-1}}$ because the infall is supersonic. Also, the photospheric component has a lower effective temperature $T_{eff} \propto R_p^{-1/2}$.

Could this apply to PDS 70 b? H19 reported a spectral width slightly above $100 \, \mathrm{km \, s^{-1}}$. The Hα from a weak shock is at least 3 times narrower, which seems inconsistent with these observations, but the measured width might be overestimated because it is comparable to the instrumental resolution (Th19; Hashimoto et al. 2020). However, Wang et al. (2021) obtained a photospheric radius $R_p \approx 2 \, R_J$. Therefore, a very weak shock seems unlikely for PDS 70 b.

4. Summary and Discussion

We have considered the predictions of the Hα flux from sophisticated non-LTE models of the postshock emission from Aoyama et al. (2018) as applied to the scenario that the shock occurs on the planet surface, as in Aoyama & Ikoma (2019). Using a broad range of $\dot{M}$ and M_p relevant for forming planets, we have shown for the first time the $L_{acc}–L_{H\alpha}$ relation for the planetary-surface shock, comparing to previously used stellar relationships (Figure 1). Appendix C extends this to other hydrogen lines. We then compared our $\dot{M}–L_{H\alpha}$ relationship to that of Thanathibodee et al. (2019). Finally, we put in perspective accretion contexts that can lead to Hα emission (Section 3).

In summary:

1. The relationship $\log(L_{acc}/L_\odot) = 0.95 \log(L_{H\alpha}/L_\odot) + 1.61$ (Equation (1)) is markedly higher at a given $L_{H\alpha}$ than extrapolating the stellar relationships from Rigliaco et al. (2012) and Alcalá et al. (2014, 2017). Thus, Hα production is less efficient for planets (Figure 1).

2. For magnetospheric accretion, the contribution of heated accretion columns (Thanathibodee et al. 2019) dominates at high $\dot{M}$, whereas the surface-shock contribution is larger at low $\dot{M}$. Whether for realistic $\dot{M}$ the emission from the column will ever dominate, however, depends on the highly uncertain temperature in that model, and presumably also on mass and radius. PDS 70 b happens

---

[14] As SzE20 write, the planet might not accrete all the mass inflowing toward the CPD, leading to the distinction between "influx" and "accretion."

to be in the intermediate-$\dot{M}$ regime (Figure 2), if the accretion funnels are hot enough to emit Hα.

3. A non-Gaussian Hα wing or a wider profile on the blue side indicates that a hot accretion funnel (Thanathibodee et al. 2019) contributes to the line, in addition to the shock-heated gas on the planetary surface (Aoyama & Ikoma 2019; Aoyama et al. 2020; Section 3.1). A weak shock on a large planet (tens of R_J) should have a narrow line (Section 3.3).

4. Importantly, we have argued (Section 3.3) that the hydrogen-line emission from large planets cannot be calculated by applying Storey & Hummer (1995) on the output of LTE, relatively low-resolution (compared to the disequilibrium microphysical processes in the postshock cooling region) radiation-hydrodynamical simulations such as those of Marleau et al. (2017, 2019) or Szulágyi & Ercolano (2020).

The new L_{acc}–$L_{\mathrm{H}\alpha}$ relationship has important implications. One is that PDS 70 b is now predicted to have $L_{\mathrm{acc}} \approx 5 \times 10^{-5} L_{\odot}$ (see Figure 1) instead of 10 to 100 times smaller using the extrapolated stellar relationships. Also, Zurlo et al. (2020) reached an average Hα upper limit of $L_{\mathrm{H}\alpha} \approx 5 \times 10^{-7} L_{\odot}$ beyond $\approx 0\farcs1$ in their survey. Using the Rigliaco et al. (2012) relationship, this would translate to $L_{\mathrm{acc}} < 4 \times 10^{-7} L_{\odot}$, while we find instead $L_{\mathrm{acc}} < 3 \times 10^{-5} L_{\odot}$, a much looser constraint. Finally, Close (2020) estimated the future observability of Hα-emitting planets but based on the R12 scaling. Using instead ours, we estimate from his Figure 8 that a large fraction of the planets should remain detectable thanks to the high assumed $\dot{M}$, where both scalings differ only by $\lesssim 1$ dex.

Finally, some words about extinction. Apart from the ISM, the matter either in the accretion flow onto the planet or in the PPD layers above the planet can contribute to the extinction. Szulágyi et al. (2019) and Sanchis et al. (2020) argued that extinction by circumstellar and circumplanetary materials could make planets or their CPDs more challenging to detect. This seems qualitatively realistic, but the extent depends strongly on the details of the accretion flow, which are heavily influenced by the numerical resolution, and on the uncertain dust properties.

We did not consider extinction by the gas nor the dust around the planet. This should be justified toward low $\dot{M}$, and for the dust it will hold especially if accreting planets are found in gaps (Close 2020), where the local dust-to-gas ratio is much lower than the global average (e.g., Drążkowska et al. 2019). Since extinction decreases the observed flux, the true $L_{\mathrm{H}\alpha}$ is higher than the $L_{\mathrm{H}\alpha}$ estimated from the observed flux. Therefore, our relationship is robustly a *lower bound* on the L_{acc} implied by the observed Hα flux. Depending on the details of the accretion and viewing geometries, heavy extinction could be avoided. To assess this observationally, comparing theoretical predictions of line ratios to simultaneous observations of several accretion tracers (Hashimoto et al. 2020) seems a promising avenue.

Appendix A
Error Bars on the Relationships

The formal statistical error bars on the fit parameters a and b are usually taken to derive error bars on the derived L_{acc} (or $\dot{M}$; see below). For a general fit $\log(L_{\mathrm{acc}}/L_{\odot}) = a \log(L_{\mathrm{H}\alpha}/L_{\odot}) + b$, the spread $\sigma_{\log L_{\mathrm{acc}}}$ for the underlying distribution of parameters is given by the standard propagation of errors:

$$\sigma_{\log L_{\mathrm{acc}}} = \sqrt{\sigma_a^2 \log(L_{\mathrm{H}\alpha})^2 + \sigma_b^2 + a^2 \sigma_{\log L_{\mathrm{H}\alpha}}^2}, \quad (A1)$$

where $\sigma_{a,\,b,\,L_{\mathrm{H}\alpha}}$ are respectively the uncertainties on a, b, and $L_{\mathrm{H}\alpha}$. With this, $L_{\mathrm{acc}} \times 10^{\pm \sigma_{\log L_{\mathrm{acc}}}}$ gives the 1σ range of values at a given $L_{\mathrm{H}\alpha}$.

The use of $\sigma_{a,b}$ implicitly assumes that the underlying relationship between $L_{\mathrm{H}\alpha}$ and L_{acc} has no intrinsic spread, with some unknown, nuisance parameter(s) leading to noise in the "observed" (from data or models) L_{acc}. Our $\sigma_{a,b}$ are much smaller than those of the literature relationships only because we use more model points for the fit than data points were used. However, in reality the spread arises because both $L_{\mathrm{H}\alpha}$ and L_{acc} depend on a number of physical parameters ($\dot{M}$, M_{p}, R_{p}) in general in a different way. Thus, it would be more appropriate to use the spread of the points σ than the formal error, contrary to what has been done up to now.

As an example, for the Al17 fit, the formal uncertainty on L_{acc} from $\log(L_{\mathrm{H}\alpha}/L_{\odot}) = -6.805 \pm 0.095$ (for PDS 70 b; H19) is $\sigma^{\mathrm{form}} = 0.11$ dex, with the contributions from the formal errors on a and b dominating. Meanwhile, the spread in the original data, which reaches down only to $\log(L_{\mathrm{H}\alpha}/L_{\odot}) \approx -6$, is rather $\sigma \approx 0.5$ dex at the low end, and mostly $\sigma \approx 0.7$ dex over the whole range. Thus, using only the formal error bars strongly underestimates the uncertainty in the derived L_{acc}. The same conclusion is reached when considering R12 and Alcalá et al. (2014), for both of which the spread of L_{acc} is $\sigma \approx 0.5$ dex over their range.

Appendix B
A Comment on Zhu (2015)

Zhu (2015) presented an expression for the Hα luminosity from accreting planets in the context of magnetospheric accretion (his Equation (21)):

$$L_{\mathrm{H}\alpha} = 4\pi R_{\mathrm{trunc}}^2 \times \pi B_{\nu}(8000\,\mathrm{K}, \nu_{\mathrm{H}\alpha}) \times \frac{v_{\mathrm{ff}}}{c} \nu_{\mathrm{H}\alpha}, \quad (B1)$$

where $B_{\nu}(T, \nu)$ is the Planck function, R_{trunc} is the magnetospheric truncation radius (Königl 1991), $\nu_{\mathrm{H}\alpha}$ is the Hα frequency, and c is the speed of light. This is meant not as a precise calculation but as a rough upper limit. Still, we comment on its applicability to put it in context.

Equation (B1) assumes that the surface of the magnetosphere is covered by an optically thick layer of hot ($T \approx 8000$ K) gas, and that the atomic hydrogen level populations are in thermal

collisional equilibrium, i.e., given by the Boltzmann distribution at the gas temperature T. This will likely hold since the freefall time is long compared to the thermal timescale, so that the radiation and gas temperatures become equal. Then if the emitting region is optically thick, the sphere of radius $R_{\rm trunc}$ emits Hα following the Planck function at this T. The densities could be such that the gas is optically thick (Zhu 2015), but a realistic geometry should lead to a smaller emitting area. Thus, the first two factors of Equation (B1) are upper limits.

The last factor in Equation (B1) assumes that the line width is equal to the infall velocity, as the magnetospheric accretion model (e.g., Hartmann et al. 1994) suggests, and assumes a top-hat line shape, i.e., that the gas is optically thick (so that the line is saturated) within $\sim v_{\rm ff}$ of $\nu_{\rm H\alpha}$ and thin outside. While this line width is consistent with the velocity distribution of the accretion funnel, the width from each region is represented by the thermal Doppler width rather than $v_{\rm ff}$. Therefore, the Doppler width is more realistic, while $v_{\rm ff}$ is better to make sure the estimate is truly an upper limit.

In summary, Equation (22) of Zhu (2015) represents a very conservative upper limit to the Hα flux expected from magnetospherically accreting planets. In our model, most Hα emission does typically come from regions at $T \approx (1\text{--}2) \times 10^4$ K. However, the Hα is usually optically thin there, making Equation (B1) really an upper limit. Indeed, for the input grid of models in Figure 1, it predicts $L_{\rm H\alpha} \lesssim 10^{-3} L_\odot$, independently of $\dot{M}$. Comparing to Figure 1, this certainly holds.

Finally, based on their nondetections, Zurlo et al. (2020) derived an upper limit on the planetary mass from the upper limit of $v_{\rm ff}$ derived with Equation (B1)[15] but not the gas temperature near the planet; for the latter, see Equation (33) of Marleau et al. (2019). However, while Equation (B1) gives an upper limit of $L_{\rm H\alpha}$ for a given planetary mass, the equation does not necessarily give an upper limit of planetary mass for a given $L_{\rm H\alpha}$. It would be interesting to repeat their analysis using more detailed models.

Appendix C
Correlation between the Line and Accretion Luminosities for Other Lines

As in Appendix E of Alcalá et al. (2017), we provide fits to the relationship between the line luminosity $L_{\rm line}$ and the accretion luminosity $L_{\rm acc}$ in our model for several hydrogen lines other than Hα, including near-infrared lines. We consider Lyα, Lyβ, Lyγ, and the transitions up to an upper level $n_{\rm up} = 8$ in the Balmer (H), Paschen (Pa), and Brackett (Br) series. Given that we include in our model lines only up to $n_{\rm up} = 10$ (Aoyama et al. 2018), these fluxes should be reliable. As in Equation (1), we write

$$\log_{10}(L_{\rm acc}/L_\odot) = a \times \log_{10}(L_{\rm line}/L_\odot) + b. \quad (C1)$$

We use the same grid of $(\dot{M}, M_{\rm p}, f_{\rm fill})$ values as in Section 2.1, and also perform straightforward least-squares fitting with `gnuplot`'s built-in `fit` function. As for Hα, we use for the fit for each line the points at $L_{\rm acc} \leqslant 10^{-4} L_\odot$. For the Lyman-series lines and the α lines of the other series, this excludes the region with a large spread in $L_{\rm acc}$ at a given $L_{\rm line}$. For the other lines, which are optically thinner, this restriction does not change the

Table 1
Relationships between Line and Accretion Luminosities

Line	λ (μm)	PMCs (This Work)			CTTSs		
		a	b (dex)	s (dex)	a	b (dex)	s (dex)
Lyα	0.121	0.90	0.43	0.24	⋯	⋯	⋯
Lyβ	0.103	0.86	0.83	0.21	⋯	⋯	⋯
Lyγ	0.097	0.86	1.17	0.21	⋯	⋯	⋯
Hα	0.656	0.95	1.61	0.11	1.13	1.74	0.41
Hβ	0.486	0.87	1.47	0.12	1.14	2.59	0.30
Hγ	0.434	0.85	1.60	0.14	1.11	2.69	0.29
Hδ	0.410	0.84	1.77	0.15	1.07	2.64	0.32
H7	0.397	0.83	1.91	0.15	1.06	2.69	0.32
H8	0.389	0.83	2.04	0.16	1.06	2.73	0.30
Paα	1.875	0.93	2.49	0.10	⋯	⋯	⋯
Paβ	1.282	0.86	2.21	0.12	1.06	2.76	0.45
Paγ	1.094	0.85	2.28	0.14	1.24	3.58	0.36
Paδ	1.005	0.84	2.38	0.15	1.22	3.74	0.40
Pa8	0.954	0.83	2.49	0.15	1.09	3.19	0.42
Brα	4.051	0.94	3.32	0.10	1.81	6.45	0.1
Brβ	2.625	0.87	2.88	0.12	⋯	⋯	⋯
Brγ	2.166	0.85	2.84	0.14	1.19	4.02	0.45
Brδ	1.944	0.84	2.88	0.15	⋯	⋯	⋯

Note. Coefficients pertain to $\log_{10}(L_{\rm acc}/L_\odot) = a \times \log_{10}(L_{\rm line}/L_\odot) + b$ as in Equation (1). PMCs: planetary-mass companions. CTTSs: classical T Tauri stars. Air wavelengths are reported, except for Lyman lines (vacuum). The CTTS fits are from Alcalá et al. (2017), except for Brα, from KF20. The s values are the standard deviations of the linear fits (estimated by eye for KF20; $N = 7$ data points). This is not the spread of the data, which is for example $\pm \sigma = \pm 0.3$ dex for our Hα line and at most 0.5 dex for some of the other lines (see Figures 3–5).

fit much and only effectively adds some statistical weight to the lower luminosities.

The fit coefficients are reported in Table 1 and compared to the stellar case. Where available, the latter are from Alcalá et al. (2017) with the exception of Brα, from Komarova & Fischer (2020, hereafter KF20). Our coefficients are mostly slightly sublinear ($a \approx 0.9$), with a flattening (smaller a) toward higher-energy transitions within each series. This holds also in the Balmer series for stars but not in the Paschen series. The σ give the standard deviation of the model points (or the data, for the CTTS column) with respect to the fit, but note that the spread of the points is larger (see discussion in Appendix A).

All these lines should trace accretion, contrary to the case for CTTSs, where other processes can alter several lines (including, in fact, Hα, which led Alcalá et al. 2017 not to recommend it as an accretion tracer). However, for any line to be observable as a shock excess, it must be stronger than the local (pseudo)continuum if the observations do not resolve it, or higher than the "noise" (i.e., the rms level) of the (pseudo)continuum for spectrally resolved observations. Being at short wavelengths $\lambda \approx 300\text{--}400$ nm, lines such as Hγ and higher-order Balmer lines are difficult to observe with existing instruments but they are included for completeness. The Lyα line is also not likely to be observed but is relevant in thermochemical models (e.g., Rab et al. 2019). The James Webb Space Telescope (JWST) should observe Brα as KF20 pointed out, and Integral Field Unit of the planned second-generation High Resolution Spectrograph on the Extremely

---

[15] The upper value of $T \sim 10^8$ K quoted by Zurlo et al. (2020) above their Equation (2) for the shock temperature in AIT18 is only the *nonequilibrium* value in extreme cases in a thin layer.

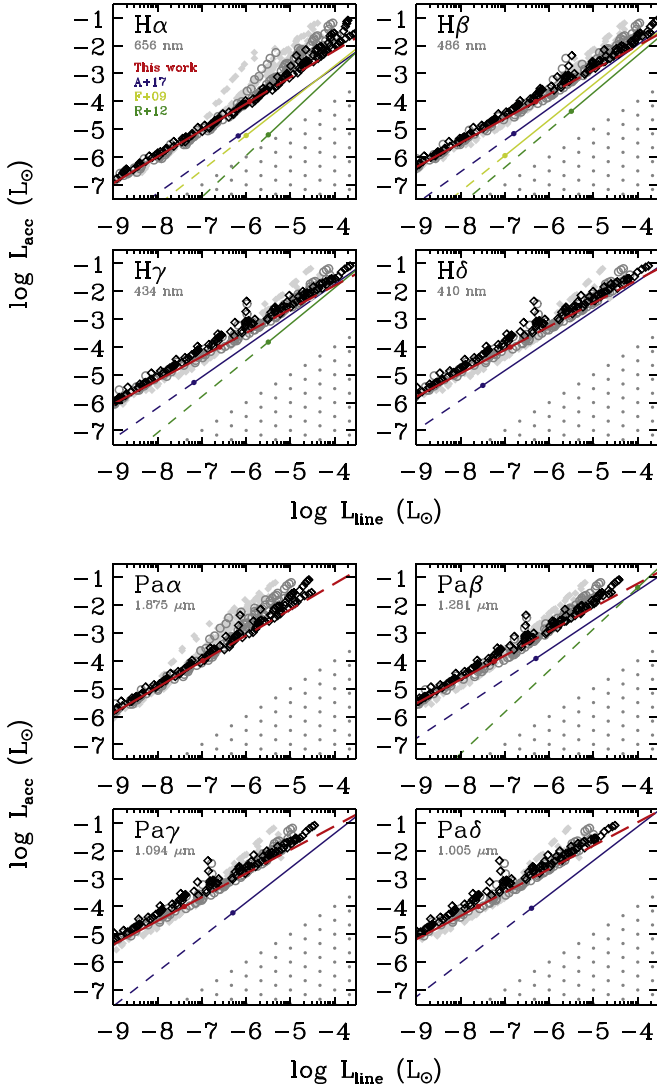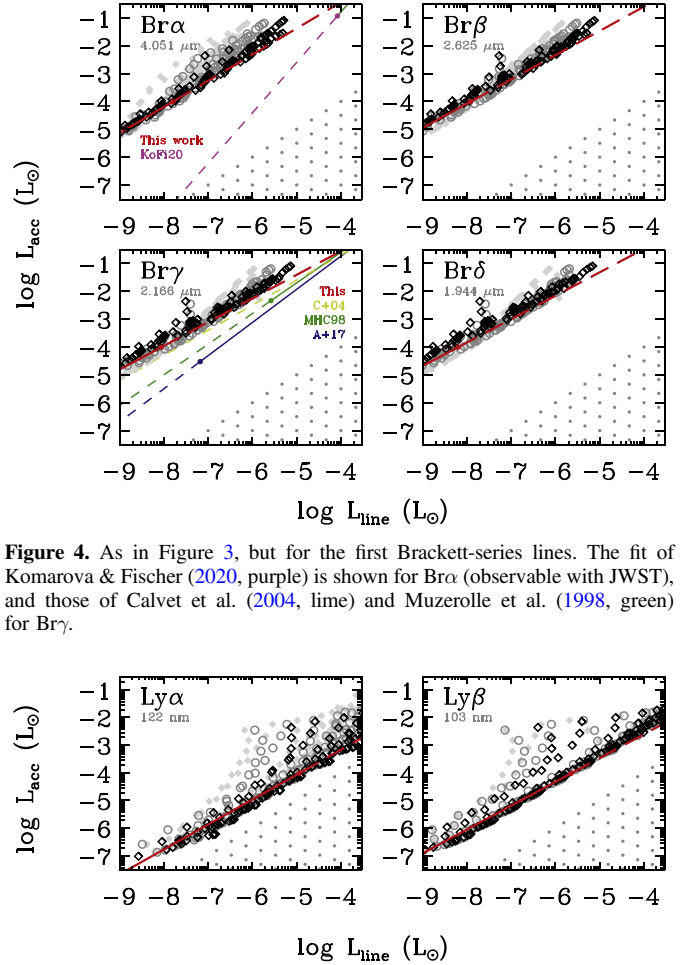**Figure 3.** Correlation between line and accretion luminosities for hydrogen lines (see labels). Symbols show our model for the same $\dot{M}$ and $M_{\rm p}$ as in Figure 1 for $f_{\rm fill} = 1$, 0.1, and 0.01 (black, dark gray, and pale gray symbols, respectively) along with the fit (red line; Table 1) from the points with $L_{\rm acc} \leqslant 10^{-4}\,L_{\odot}$ (solid). Where available, the fits of Alcalá et al. (2017, blue), Fang et al. (2009, lime), and Rigliaco et al. (2012, green) are shown (solid: where their data exist; dashed: extrapolation). A dot marks the transition between fits and extrapolations but in our case the latter hold everywhere as a lower limit. In the dotted region, $L_{\rm line} > L_{\rm acc}$, which is likely unphysical (see Section 2.1).

Figure 4. As in Figure 3, but for the first Brackett-series lines. The fit of Komarova & Fischer (2020, purple) is shown for Brα (observable with JWST), and those of Calvet et al. (2004, lime) and Muzerolle et al. (1998, green) for Brγ.
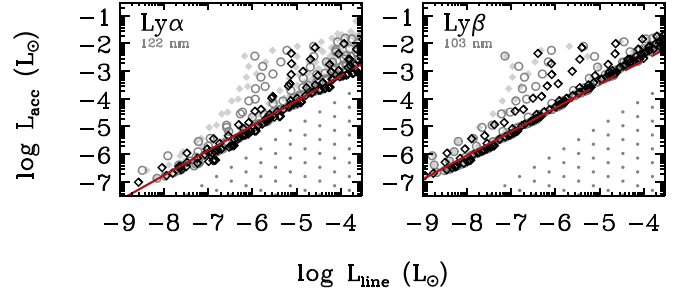
Figure 5. As in Figure 3, but for Lyα and Lyβ. Lyman-series lines are less reliable than the others but are shown for completeness.

Large Telescope (ELT), expected to come online in the next decade, will cover 1.0–1.8 μm, which includes several of the other lines. Its tremendous resolution of $R \approx 100{,}000$–150,000 should allowed detailed studies of the kinematics of the infalling gas.

Figures 3–5 show our model results and the fits for several lines from the Balmer (Hα, Hβ, Hγ, Hδ; upper panels in Figure 3), Paschen (Paα, Paβ, Paγ, Paδ; lower panels in Figure 3), and Brackett (Brα, Brβ, Brγ, Brδ; Figure 4) series, and also from the Lyman series (Lyα, Lyβ; Figure 5). In all cases, the fit to our results (red line) is roughly a lower limit. For the chosen range of input planet masses (2–20 $M_{\rm J}$) and excluding the Lyman-series lines, the half-spread in $L_{\rm acc}$ at a given $L_{\rm line}$ is often relatively small, with $\sigma \approx 0.3$ dex, but can reach $\sigma \approx 0.5$ dex. For the Lyman lines, the high optical depth of the upper layers of the postshock region lead to strong self-absorption. This is especially true for the points for lower planet masses, which have a higher density at a given $\dot{M}$ since $\rho \propto 1/v_{\rm ff}$.

For all transitions, our data are above the stellar relationship, for the $L_{\rm line}$ values covered both by their data and our model results, as well as where the stellar fit is extrapolated. The difference reaches up to 1–2 dex for the Balmer lines, especially compared to Rigliaco et al. (2012), and 2–3 dex for Paschen lines. For Brα, the difference is extreme (2–4 dex) compared to the fit of Komarova & Fischer (2020). This is however not surprising because there is barely an overlap in $L_{\rm acc}$ between their data and our models, and their fit does not cover at all the $L_{\rm line}$ values relevant to planetary accretion ($L_{\rm line} \lesssim 10^{-5.5}\,L_{\odot}$). In general, as discussed in Section 2.1, we do not expect the $L_{\rm acc}$–$L_{\rm line}$ relationships to match between the stellar and planetary regimes because the generating mechanisms probably differ significantly. Note that, except for the Hα fit of Rigliaco et al. (2012), none of the extrapolations of the stellar fits reaches into the $L_{\rm line} > L_{\rm acc}$ region, which would be likely unphysical (Section 2.1).

ORCID iDs

Yuhiko Aoyama ⓘ https://orcid.org/0000-0003-0568-9225
Gabriel-Dominique Marleau ⓘ https://orcid.org/0000-0002-2919-7500

Masahiro Ikoma ⬤ https://orcid.org/0000-0002-5658-5971
Christoph Mordasini ⬤ https://orcid.org/0000-0002-1013-2811

References

Alcalá, J. M., Manara, C. F., Natta, A., et al. 2017, A&A, 600, A20
Alcalá, J. M., Natta, A., Manara, C. F., et al. 2014, A&A, 561, A2
Aoyama, Y., & Ikoma, M. 2019, ApJL, 885, L29
Aoyama, Y., Ikoma, M., & Tanigawa, T. 2018, ApJ, 866, 84
Aoyama, Y., Marleau, G.-D., Mordasini, C., & Ikoma, M. 2020, arXiv:2011.06608
Batygin, K. 2018, AJ, 155, 178
Brittain, S. D., Najita, J. R., Dong, R., & Zhu, Z. 2020, ApJ, 895, 48
Calvet, N., & Gullbring, E. 1998, ApJ, 509, 802
Calvet, N., Muzerolle, J., Briceño, C., et al. 2004, AJ, 128, 1294
Christensen, U. R., Holzwarth, V., & Reiners, A. 2009, Natur, 457, 167
Close, L. M. 2020, AJ, 160, 221
Cugno, G., Quanz, S. P., Hunziker, S., et al. 2019, A&A, 622, A156
Dong, J., Jiang, Y.-F., & Armitage, P. 2020, arXiv:2012.06641
Drążkowska, J., Li, S., Birnstiel, T., Stammler, S. M., & Li, H. 2019, ApJ, 885, 91
Eriksson, S. C., Asensio Torres, R., Janson, M., et al. 2020, A&A, 638, L6
Fang, M., van Boekel, R., Wang, W., et al. 2009, A&A, 504, 461
Gravity Collaboration, Garcia Lopez, R., Natta, A., et al. 2020, Natur, 584, 547
Gullbring, E., Hartmann, L., Briceño, C., & Calvet, N. 1998, ApJ, 492, 323
Haffert, S. Y., Bohn, A. J., de Boer, J., et al. 2019, NatAs, 3, 749
Hartmann, L., Herczeg, G., & Calvet, N. 2016, ARA&A, 54, 135
Hartmann, L., Hewett, R., & Calvet, N. 1994, ApJ, 426, 669
Hashimoto, J., Aoyama, Y., Konishi, M., et al. 2020, AJ, 159, 222
Herczeg, G. J., Wood, B. E., Linsky, J. L., Valenti, J. A., & Johns-Krull, C. M. 2004, ApJ, 607, 369
Hummer, D. G., & Storey, P. J. 1987, MNRAS, 224, 801
Ingleby, L., Calvet, N., Herczeg, G., et al. 2013, ApJ, 767, 112
Komarova, O., & Fischer, W. J. 2020, RNAAS, 4, 6
Königl, A. 1991, ApJL, 370, L39
Landsman, W., & Simon, T. 1993, ApJ, 408, 305
Lovelace, R. V. E., Covey, K. R., & Lloyd, J. P. 2011, AJ, 141, 51

Lubow, S. H., & Martin, R. G. 2012, ApJL, 749, L37
Marleau, G.-D., Aoyama, Y., Kuiper, R., et al. 2021, A&A, submitted
Marleau, G.-D., Klahr, H., Kuiper, R., & Mordasini, C. 2017, ApJ, 836, 221
Marleau, G.-D., Mordasini, C., & Kuiper, R. 2019, ApJ, 881, 144
Martin, S. C. 1996, ApJ, 470, 537
Mordasini, C., Alibert, Y., Georgy, C., et al. 2012, A&A, 547, A112
Mordasini, C., Marleau, G.-D., & Mollière, P. 2017, A&A, 608, A72
Muzerolle, J., Calvet, N., & Hartmann, L. 1998, ApJ, 492, 743
Muzerolle, J., Calvet, N., & Hartmann, L. 2001, ApJ, 550, 944
Owen, J. E., & Menou, K. 2016, ApJL, 819, L14
Rab, C., Kamp, I., Ginski, C., et al. 2019, A&A, 624, A16
Rigliaco, E., Natta, A., Testi, L., et al. 2012, A&A, 548, A56
Sallum, S., Follette, K. B., Eisner, J. A., et al. 2015, Natur, 527, 342
Sanchis, E., Picogna, G., Ercolano, B., Testi, L., & Rosotti, G. 2020, MNRAS, 492, 3440
Schulik, M., Johansen, A., Bitsch, B., & Lega, E. 2019, A&A, 632, A118
Schulik, M., Johansen, A., Bitsch, B., Lega, E., & Lambrechts, M. 2020, A&A, 642, A187
Storey, P. J., & Hummer, D. G. 1995, MNRAS, 272, 41
Szulágyi, J., Dullemond, C. P., Pohl, A., & Quanz, S. P. 2019, MNRAS, 487, 1248
Szulágyi, J., & Ercolano, B. 2020, ApJ, 902, 126
Szulágyi, J., Morbidelli, A., Crida, A., & Masset, F. 2014, ApJ, 782, 65
Szulágyi, J., & Mordasini, C. 2017, MNRAS, 465, L64
Tanigawa, T., & Ikoma, M. 2007, ApJ, 667, 557
Tanigawa, T., Ohtsuki, K., & Machida, M. N. 2012, ApJ, 747, 47
Teague, R., Bae, J., & Bergin, E. A. 2019, Natur, 574, 378
Thanathibodee, T., Calvet, N., Bae, J., Muzerolle, J., & Hernández, R. F. 2019, ApJ, 885, 94
Wagner, K., Follete, K. B., Close, L. M., et al. 2018, ApJL, 863, L8
Wang, J. J., Vigan, A., Lacour, S., et al. 2021, AJ, 161, 148
Xie, C., Haffert, S. Y., de Boer, J., et al. 2020, A&A, 644, A149
Zhou, Y., Bowler, B. P., Wagner, K. R., et al. 2021, AJ, 161, 244
Zhou, Y., Herczeg, G. J., Kraus, A. L., Metchev, S., & Cruz, K. L. 2014, ApJL, 783, L17
Zhu, Z. 2015, ApJ, 799, 16
Zurlo, A., Cugno, G., Montesinos, M., et al. 2020, A&A, 633, A119